

**Materials Corrosion and Mitigation Strategies for APT,
End of FY '97 Report:**

**II. Out-of-Beam Corrosion Rates and Water Analysis from the
'97 A6 Irradiation**

R. Scott Lillard, Donald L. Pile, Darryl P. Butt

Materials Corrosion & Environmental Effects Lab
MST-6, Metallurgy Group
Los Alamos National Laboratory, Los Alamos NM 87545

August 1, 1998

submitted to:

Laurie Waters
APT - Technical Project Office
Los Alamos National Laboratory
Los Alamos, NM 87545

contributors:

Walter Sommer, APT-TPO
Stuart Maloy, APT-TPO
Gordon Willcutt, TSA-10
Richard Werbeck, LANSCE-7
Robert Brown, LANSCE-7
Eugene Zimmermann, NMT-11

Summary of FY 1997 Accomplishments

The Corrosion sub-group of the APT Materials Irradiation Team successfully met all of its FY 1997 deliverables. The following is an abbreviated list of these accomplishments and some of those in FY '98:

LANSCE-A6 Experiments:

- 1) design, procurement, and testing of in-beam corrosion probes with ceramic feed-through
- 2) procurement and testing of all other probes in the system including out-of-beam probes, hydrogen sensor, pH probes, conductivity probes
- 3) fabrication of water system and manifold for A6 experiments (with LANSCE-7)
- 4) pre-irradiation testing of the A6 corrosion loop, associated equipment, and probes
- 5) measurement of in-beam corrosion rate for IN718 as a function of proton beam current
- 6) long term measurement of in-beam corrosion rate for IN718 at 1 mA
- 7) measurement of out-of-beam corrosion rates for IN718, SS304L, SS316L, Al6061, Al5052, W, and Ta in an irradiated water system
- 8) analysis and computer modeling of in-beam corrosion data
- 9) analysis and computer modeling of out-of-beam corrosion data
- 10) LA-UR # 97-0561, "Using Solution Resistivity as an Estimate of Tungsten Corrosion in Spallation Neutron Target Cooling Loops", by R.S. Lillard and D.P. Butt. (internal report)
- 11) LA-UR# 97-3854, "The Susceptibility of Materials in Spallation Neutron Source Target and Blanket Cooling Loops to Corrosion", by R.S. Lillard and D.P. Butt. (submitted to *Materials Characterization* for consideration in the APT Review Article)
- 12) LA-UR# 98-0764, "Materials Corrosion and Mitigation Strategies for APT, End of FY '97 Report: I. Inconel 718 In-Beam Corrosion Rates from the '97 A6 Irradiation", by R.S. Lillard, D.L. Pile, D. P. Butt. (internal report)
- 13) LA-UR# 97-XXX, "Materials Corrosion and Mitigation Strategies for APT, End of FY '97 Report: II. Out-of-Beam Corrosion Rates and Water Analysis from the '97 A6 Irradiation", by R.S. Lillard, D.L. Pile, D. P. Butt. (internal report)

WNR Experiments:

Nov. 1996

- 1) design and fabrication of in-beam corrosion loop for use at WNR
- 2) in-beam corrosion rate measurements for tungsten as a function of beam current
- 3) analysis and computer modeling of in-beam tungsten data from WNR experiments
- 4) LA-UR# 97-3134, "Corrosion of Tungsten in an 800 MeV Proton Beam at the Weapons Neutron Research Facility", R.S. Lillard, D.P. Butt, (internal report).

June 1997

- 5) in-beam electrochemical experiments on W, Ta, SS304L, and Au as a function of beam current
- 6) in-beam Surface Enhanced Raman experiments of the passive oxide on W as a function of beam current
- 7) LA-UR# 97-5011, "Materials Corrosion and Mitigation Strategies for APT, Weapons Neutron Research Facility Experiments: The Effects of 800 MeV Proton Irradiation on the Corrosion of Tungsten, Tantalum, Stainless Steel, and Gold", R.S. Lillard, D.P. Butt, G. Kanner, L. Daemen. (internal report).

Laboratory Experiments

- 1) W corrosion rate measurements as a function of solution composition and pH
- 2) surface enhanced Raman measurements of the W passive oxide as a function of solution pH
- 3) LA-UR# 98-0631, "The Nature of Oxides on Tungsten in Acidic and Alkaline Solutions and Their Role in the Dissolution Process", R.S. Lillard, G.S. Kanner, D.P. Butt. (accepted for publication in *The Journal of the Electrochemical Society*).

Executive Summary

The corrosion rates for Inconel 718, stainless steels 304L and 316NUC, aluminum alloys 5052 and 6061, tantalum, and tungsten in water irradiated by the 800 MeV proton beam at the LANSCE A6 target station are reported. These real-time corrosion rates were measured during the FY '97 irradiation period between March and July of 1997 in the APT-Corrosion water loop. This report also details our efforts to quantify water quality as a function of irradiation time. In these efforts, we have monitored water conductivity, isotopic abundance (via gamma analysis), and heavy metal concentrations (via ICP). In an attempt to mitigate corrosion, hydrogen has been bubbled into the water system resulting in a dissolved hydrogen concentration of approximately 0.30 ppm. Hydrogen acts as a "getter" for some radiolysis products and limits hydrogen peroxide formation. After 131 days of irradiation the hydrogen peroxide concentration in our system was only 11.4 ppm.

Caution is warranted when evaluating the following corrosion rates. The calculations used in determining these rates yield a surface average rate and, therefore, may not be conservative. Visual observation of the probe surface to examine for localized corrosion is necessary to confirm the following rates. In addition, in the absence of dissolved hydrogen these rates will likely be higher.

The corrosion rates for the tungsten, Al5052 and Inconel 718 electrodes as a function of immersion time are presented in Figure 1.es through 3.es. The behavior of these samples was typical of the responses observed in the other materials (presented in the Results and Discussion section of this paper). The proton beam status has been divided into three separate categories in these plots: 1) pre-irradiation, beam off, 2) beam on, 0.001-0.40 mA, corrosion insert only, and 3) beam on, 1 mA, all forward inserts in place. During the early experiments when only the corrosion insert was in-beam, the beam spot at the corrosion manifold had a Gaussian distribution of $2\sigma = 3$ cm. With the forward inserts in place, because the proton beam first strikes 3 inserts before reaching the corrosion system the proton beam is no longer as focused at the corrosion insert, that is, 2σ at the corrosion manifold was greater than 3 cm. With respect to the corrosion rate of W (Figure 1.es), an increase in corrosion rate of the return side sample was observed at early immersion times. Moreover, the corrosion rate appears to increase with beam current during this time period to a maximum value of approximately $33\mu\text{m}/\text{yr}$ ($0.0013''$ per year). As no increase in the corrosion rate of the W sample on the supply side was observed in this time period, and the corrosion rate of both samples decreases after flushing and refilling the system on day 10 we may assume that this increase owes to radiolysis products in the return side of the water system which are either "consumed" or diluted sufficiently in the reserve tank before reaching the supply side probes such that no change in the corrosion rate of the W sample on the supply side was observed. Once again, during the 0-10 day time period only the corrosion insert was in place. No other inserts were in place (up stream) to diffuse the proton beam. At longer immersion times, the corrosion rate of the W sample on the return side again begins to increase. However, around 70 days of immersion a gradual decrease in corrosion rate was observed.

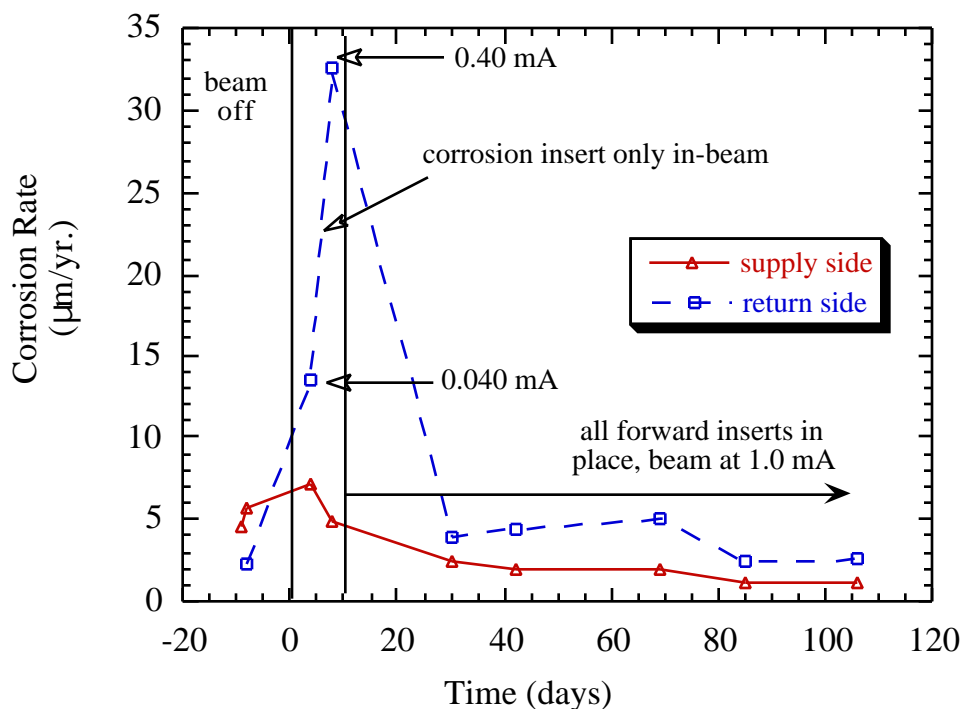


Figure 1.es Corrosion rate for the tungsten corrosion probes as a function of immersion time.

With respect to the Al alloys (Figure 2.es), the observed changes in corrosion rate for each probe as a function of immersion time appear to follow the same trend and were independent of feed solution type (supply side vs return side) and alloy type. At early immersion times (pre-irradiation) the rates were relatively high, probably due to inadequate cleaning of the water system as similar rates were observed on both the supply and return sides. In contrast to the corrosion rate of the W sample (return side), after flushing and refilling the water system on day 6 the corrosion rate decreases, even though the beam is on at low current (0.001-0.40 mA). This indicates that Al alloys are more susceptible to the make-up water's purity than radiolysis products. As observed in the W corrosion rate (return side) at longer immersion times, beam on at 1 mA, a peak in the corrosion rate around 40 days of immersion was observed again. The gradual decrease in corrosion rate after 40 days of immersion likely owes to a slow leak in the water system.

With respect to the Inconel 718, sample (Figures 3.es) no trends in corrosion rate with immersion time were observed. Moreover, the corrosion rates were extremely low, $<0.1 \mu\text{m/yr.}$; therefore, the observed changes in corrosion rate more likely owe to inaccuracies in our measurement and modeling rather than real changes in corrosion rates.

In summary, the corrosion rates for stainless steels 304L and 316NUC, Inconel 718, and tantalum were extremely low, less than $0.12 \mu\text{m/yr.}$ Although visual inspection for areas of localized corrosion is necessary, from these results we conclude that the service lifetime of these materials as it relates to corrosion in a deionized water, spallation neutron target cooling loop which employs hydrogen water chemistry would be extremely high, 20 years or more. For example, in a 10 yr. period the total Inconel 718 loss in a deionized

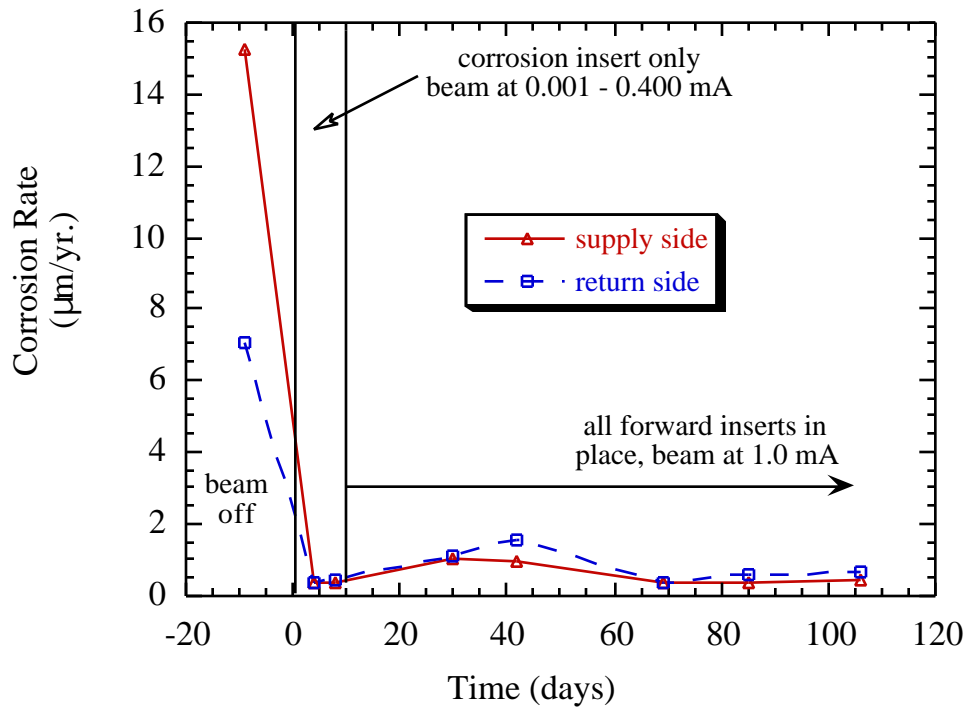


Figure 2.es Corrosion rate for aluminum alloy 5052 corrosion probes as a function of immersion time.

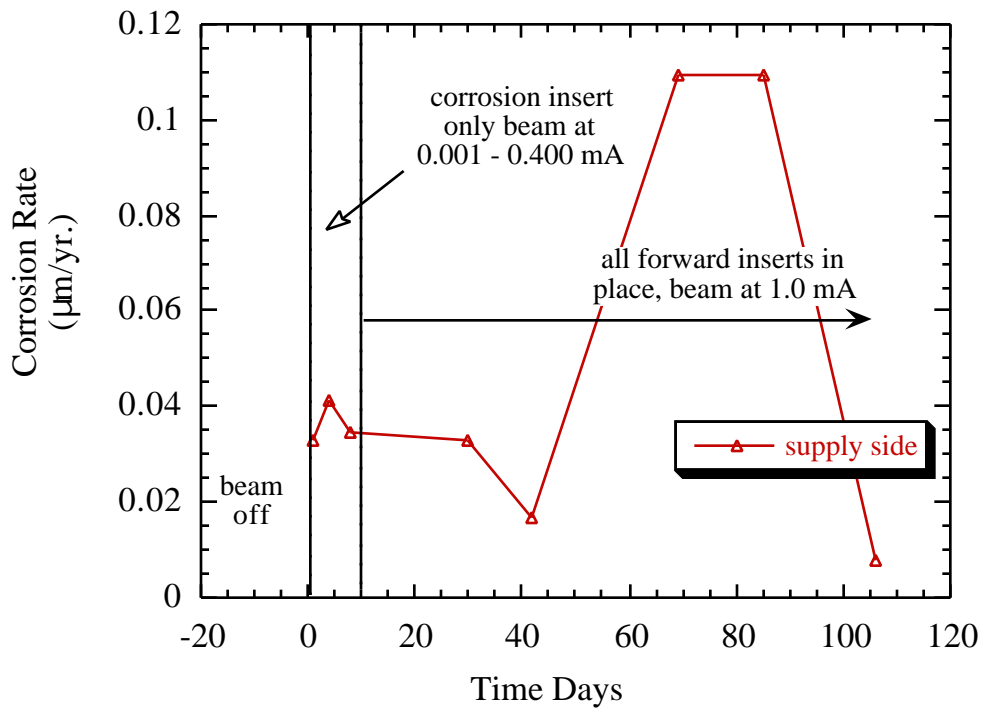


Figure 3.es Corrosion rate for the supply side 718 corrosion probe as a function of immersion time. The return side probe did not pass our certification test.

water spallation neutron target cooling loop which employs hydrogen water chemistry would be less than 0.001". For comparison, the corrosion rate of an Inconel 718 sample placed directly in the proton beam has been shown in other investigations to be greater than 0.002"/yr.

For aluminum alloys 6061 and 5052 the corrosion rates were slightly higher than the iron and nickel base alloys, on the order of 0.5 to 2.0 $\mu\text{m}/\text{yr}$. However, the service lifetime of these materials in a deionized water, spallation neutron target cooling loop which employs hydrogen water chemistry is expected to be comparable to that of the stainless steels.

Relative to the other materials tested in this investigation, the corrosion rate of tungsten was found to be high, between 5 and 30 $\mu\text{m}/\text{yr}$. However, in a 10 yr. period the total loss of material from a tungsten component in a deionized water, spallation neutron target cooling loop which employs hydrogen water chemistry due to corrosion would only be 0.002" - 0.012". For comparison, the corrosion rate of a tungsten sample placed directly in the proton beam has been shown in other investigations to be greater than 0.060"/yr.

Table of Contents

	page
Summary of FY 1997 Accomplishments	ii
Executive Summary	iii
List of Tables	viii
List of Figures	ix
Introduction	1
Background	1
<i>Water Radiolysis</i>	1
<i>Corrosion in Radiolyzed Water</i>	3
<i>Electrochemical Impedance Spectroscopy</i>	3
Experimental	4
<i>The Corrosion Loop</i>	4
<i>Out-of-Beam Corrosion Probes</i>	5
<i>Conductivity Probes</i>	7
<i>Hydrogen Water Chemistry</i>	7
Results and Discussion	8
<i>OCP Measurements</i>	8
<i>EIS Data and CNLS Modeling</i>	11
<i>Corrosion Rate vs Immersion Time</i>	14
<i>Water Resistivity and Sampling Analyses</i>	20
Summary	22
References	24

List of Tables

	page
Table 1 Elementary equations showing some of the water radiolysis products formed during irradiation, their decomposition mechanism, rate constant, and activation energy (from ref.5).	2
Table 2 Gamma and ICP analyses of water samples taken from the cooling loop as a function of time. Hydrogen peroxide concentration from paramagnetic titration is also presented. The beam was turned on at day 0, therefore, negative days indicate the period before the beam was turned on.	21

List of Figures

	page
Figure 1 Diagram representing the LANSCE A6 closed loop corrosion system. The Proton beam strikes the water loop at the base of the insert (in-beam corrosion probes). The radiolyzed water then circulates from the beam spot through the remainder of the loop including the out-of-beam probes reported on here.	5
Figure 2 A diagram of the commercially available 3-electrode corrosion probes used in the LANSCE out-of-beam corrosion measurements.	6
Figure 3 OCP of W/W-oxide electrode as a function of solution pH.	9
Figure 4 OCP of W/W-oxide and a Pt electrode as a function of time. Plot shows the effect of H ₂ and H ₂ O ₂ additions.	9
Figure 5 OCP of W and Ta electrodes in the cooling water loop (supply and return electrodes) as a function of irradiation time.	10
Figure 6 OCP of 304L, 316NUC, and 718 electrodes in the cooling water loop (supply and return electrodes) as a function of irradiation time.	10
Figure 7 OCP of the Al 5052 and 6061 electrodes in cooling water loop (supply and return electrodes) as a function of irradiation time.	11
Figure 8 Bode magnitude and phase plots for the out-of-beam Inconel 718 probe (supply side). Proton beam current was 0.04 mA when these data were collected.	12
Figure 9 Bode magnitude and phase plots for the out-of-beam W probe (return side). Proton beam current was 0.04 mA when these data were collected.	12
Figure 10a Bode magnitude plots for the out-of-beam W probe (return side) as a function of proton beam current.	13
Figure 10b Bode phase plots for the out-of-beam W probe (return side) as a function of proton beam current.	13
Figure 11 Equivalent circuits used to model EIS data: a) simplified Randles circuit and b) diffusion impedance circuit.	14
Figure 12 Corrosion rate for the tungsten corrosion probes as a function of immersion time.	16
Figure 13 Corrosion rate for aluminum alloy 5052 corrosion probes as a function of immersion time.	17
Figure 14 Corrosion rate for aluminum alloy 6061 corrosion probes as a function of immersion time.	18

Figure 15 Corrosion rate for the stainless steel 304L corrosion probes as a function of immersion time.	18
Figure 16 Corrosion rate for the stainless steel 316NUC corrosion probes as a function of immersion time.	19
Figure 17 Corrosion rate for the supply side 718 corrosion probe as a function of immersion time. The return side probe did not pass our certification test.	19
Figure 18 Corrosion rate for the tantalum corrosion probes as a function of immersion time.	20
Figure 19 Water resistivity as a function of time from both the supply and return probes.	21

Introduction

The objective of this investigation was to measure the corrosion rates of candidate stainless steel, aluminum, nickel based alloys, and refractory metals for the APT target blanket cooling loop during exposure to water irradiated by, an 800 MeV proton beam. In addition to water radiolysis products, these out-of-beam materials may be subjected to contaminants such as chloride and sulfate owing to inadequate cleaning of the system or sub-standard water purification. In this paper electrochemical impedance spectroscopy was used to measure the corrosion rate of aluminum 6061 and 5052, stainless steel 304L and 316NUC, Inconel 718, tungsten, and tantalum as a function of immersion time in water irradiated by an 800 MeV proton beam at the Los Alamos Neutron Science Center A6 Target station.

It may be noted that the materials in this investigation were not exposed to the proton beam during the course of the experiment. An investigation of the effects of proton irradiation on corrosion rate has been presented in an earlier paper(1).

Background

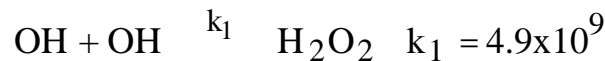
Water Radiolysis Radiolysis models(2, 3, 4) have predicted that both oxidizing and reducing species are produced when water is irradiated with proton, neutron, or gamma radiation. These species include: H_2 , O_2 , H_2O_2 , OH , H , e^-_{aq} , HO_2 , O_2^- , HO_2^- , OH^- , H^+ . A list of some of the possible decomposition mechanisms for these species and their respective rate constants are presented in Table 1. As indicated by the reaction rate constants, the lifetime of many of these species is short, on the order of microseconds to nanoseconds and with the exception of hydrogen peroxide, oxygen, and hydrogen the steady state concentration of these species is on the order of 10^{-10} to 10^{-8} M. While these short lived species may be an important consideration in the corrosion mechanism at the proton beam / metal / solution interface, i.e. the Helmholtz layer, they will have little impact on materials "downstream" in the cooling water loop.

Table 1 Elementary equations showing some of the water radiolysis products formed during irradiation, their decomposition mechanism, rate constant, and activation energy (from ref.5).

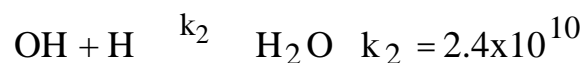
Reaction	Rate Constant (sec) ⁻¹	Activation Energy (Kcal/mol)
e ⁻ + H ₂ O = H + OH ⁻	2.4 x10 ¹⁰	3
e ⁻ + OH = OH ⁻	3.0 x10 ¹⁰	3
H + H = H ₂	1 x10 ¹⁰	3
e ⁻ + HO ₂ = HO ₂ ⁻	2 x10 ¹⁰	3
OH + OH = H₂O₂	4.5 x10⁹	3
H + OH = H₂O	2.4 x10¹⁰	3
H + O ₂ = HO ₂	1 x10 ⁹	3
OH ⁻ + H ₂ O ₂ = HO ₂ ⁻ + H ₂ O	1 x10 ⁸	4.5
HO ₂ = O ₂ ⁻ + H ⁺	8 x10 ⁵	3

Long-lived radiolysis products such as hydrogen peroxide (H₂O₂) and oxygen (O₂) are the products most likely to influence the corrosion reaction mechanism of downstream materials as they are oxidizing species(5) that have lifetimes on the order of days or weeks. At the OCP anodic and cathodic reactions on the metal surface are occurring at the same rate. As corrosion reactions are generally cathodically limited, an increase in the concentration of an oxidizing species increases the cathodic reaction and, correspondingly, increases the anodic (dissolution) reaction.

Radiolysis models have also shown that the addition of a scavenger gas (such as H₂) can greatly effect the steady state concentration of H₂O₂ and oxygen O₂ (5). For example, hydrogen peroxide is formed when two OH radicals combine:



By bubbling H₂ gas into the system the OH radical preferentially reacts with the resultant dissolved atomic hydrogen in the cooling loop to form water:



A similar reaction sequence can be written for O₂ formation and suppression. The ability of hydrogen gas to suppress the concentration of total oxidant (H₂O₂+ O₂) in a water system

exposed to radiation has long been recognized by the boiling water reactor (BWR) community. A typical BWR operates at a dissolved hydrogen concentration on the order of 50 ppb to mitigate the increased susceptibility to stress corrosion cracking that results from high concentrations of total oxidant.

Corrosion in Radiolyzed Water Investigations of the effects of radiolyzed water on corrosion rate can be divided into two general categories: 1) simulated environments and 2) experiments where the electrochemical cell containing the working electrode (or weightloss coupon) is placed in either Co^{60} or Ce^{137} sources. In this latter category of experiments the OCP of stainless steels(6) and titanium(7) have been observed to shift in the noble direction. This positive increase in the OCP has been attributed to the radiolytic production of hydrogen peroxide, in a mechanism similar to that described above. However, by the nature of their set-up these experiments expose both the water and sample to γ -radiation and, therefore, do not separate the effect of radiolysis products from those effects associated with γ -radiation. In other studies, potentiodynamic polarization curves for Ti after 12 month exposure to brine solution with γ -radiation show small decreases in anodic current densities and limited thickening of the passive film as compared to unirradiated samples(8). X-ray photoelectron spectroscopy of the passive film on stainless steel after exposure to γ -radiation found a film that was depleted in iron and enriched in chromium(9).

Electrochemical Impedance Spectroscopy (EIS) EIS is a powerful non-destructive technique for measuring the corrosion rates of metals in aqueous environments(10, 11, 12) and is ideally suited for systems with high solution resistivity. In EIS a small sinusoidal voltage perturbation (10 - 30 mV) is applied across the sample interface as a function of frequency. By measuring the transfer function of the applied ac voltage perturbation and the ac current response of the material, an impedance results ($Z = V / I$). In the simplest sense, at low frequencies the material behaves as a resistor and $Z = (R_{\text{sol}} + R_{\text{pol}})$. At high frequencies, the material behaves as a capacitor and, therefore, offers no resistance to current. As a result $Z = R_{\text{sol}}$. By measuring Z over a wide frequency range the solution

resistance can be subtracted from the polarization resistance. Because the ac voltage perturbation used in EIS is small, it is a nondestructive technique and corrosion rates can be measured at the material's "free corrosion potential" (i.e., its open circuit potential).

Experimental

The Corrosion Loop A diagram representing the LANSCE A6 Corrosion Loop is presented in Figure 1. This was a closed loop system, constructed entirely of stainless steel 304. The nominal operating pressure was 150 psi at a flow rate of 10-20 gal/min. and a temperature of 30° C. Prior to placing the corrosion probes into this system, it was steam cleaned followed by several rinsings with a 50% DI water / 50% ethanol mixture. This was followed by several rinsings with DI water. Each rinse entailed filling the expansion and reserve tanks with the solution and circulating it through the system with the pump. Each of the diagnostics that appear in Figure 1 are detailed in the following sections with the exception of the in-beam corrosion probes which have been discussed in a separate paper(1). The in-beam designation refers to corrosion probes that were placed directly in the proton beam to evaluate the effects of the beam as well as short lived radiolysis products on the corrosion rates of candidate materials.

The primary diagnostics for evaluating the corrosion rates of materials in an irradiated water only are represented in Figure 1 as "out-of-beam corrosion". The out-of-beam designation refers to samples placed in the supply stream and return stream of the flow line to evaluate the effects of long lived radiolysis products on the corrosion rates of

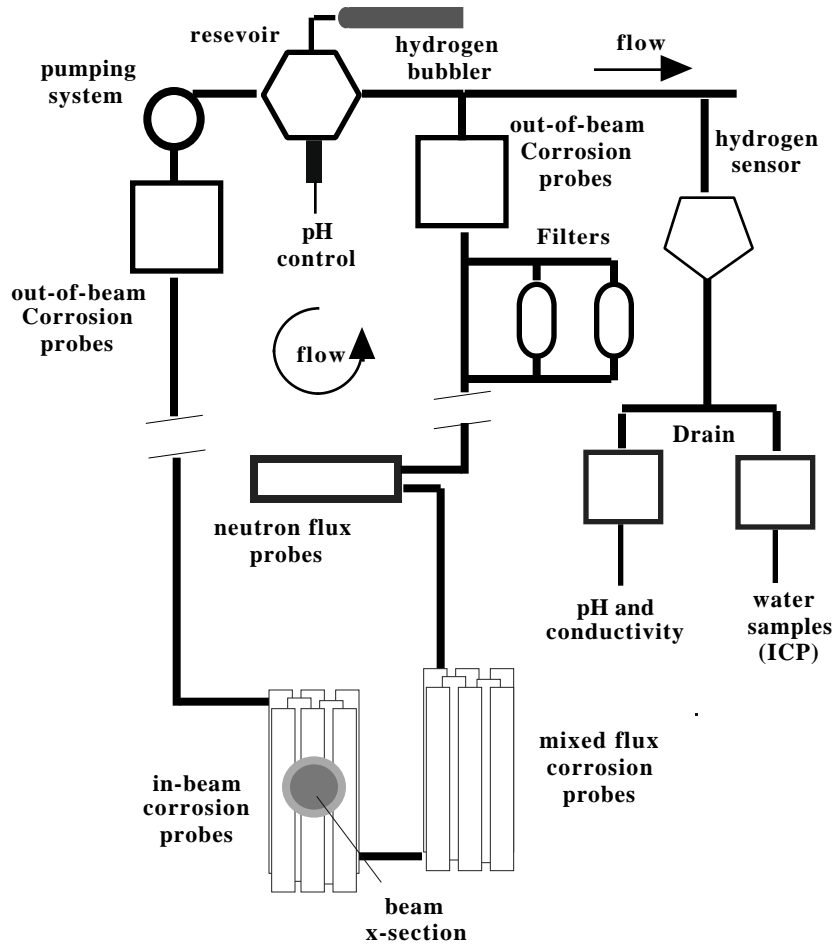


Figure 1 Diagram representing the LANSCE A6 closed loop corrosion system. Only the in-beam samples are exposed to the high energy proton. The radiolyzed water then circulates from the beam spot through the remainder of the loop.

materials. In an attempt to mitigate corrosion, hydrogen gas was bubbled into the flow stream (designated as H₂ bubbler). In addition, commercially available pH and conductivity probes were placed in the water sampling line of the system. This line was operated at system pressure.

Out-of-Beam Corrosion Probes The out-of-beam corrosion probes used in these experiments were commercially available NPT pipe plug style feed throughs which employed metal to glass seals. A diagram of these probes is shown in Figure 2. The corrosion samples were fabricated from rods approximately 0.125” in diameter by 2-3” in length of aluminum alloys 6061 and 5052, stainless steel 304L and 316NUC, tungsten,

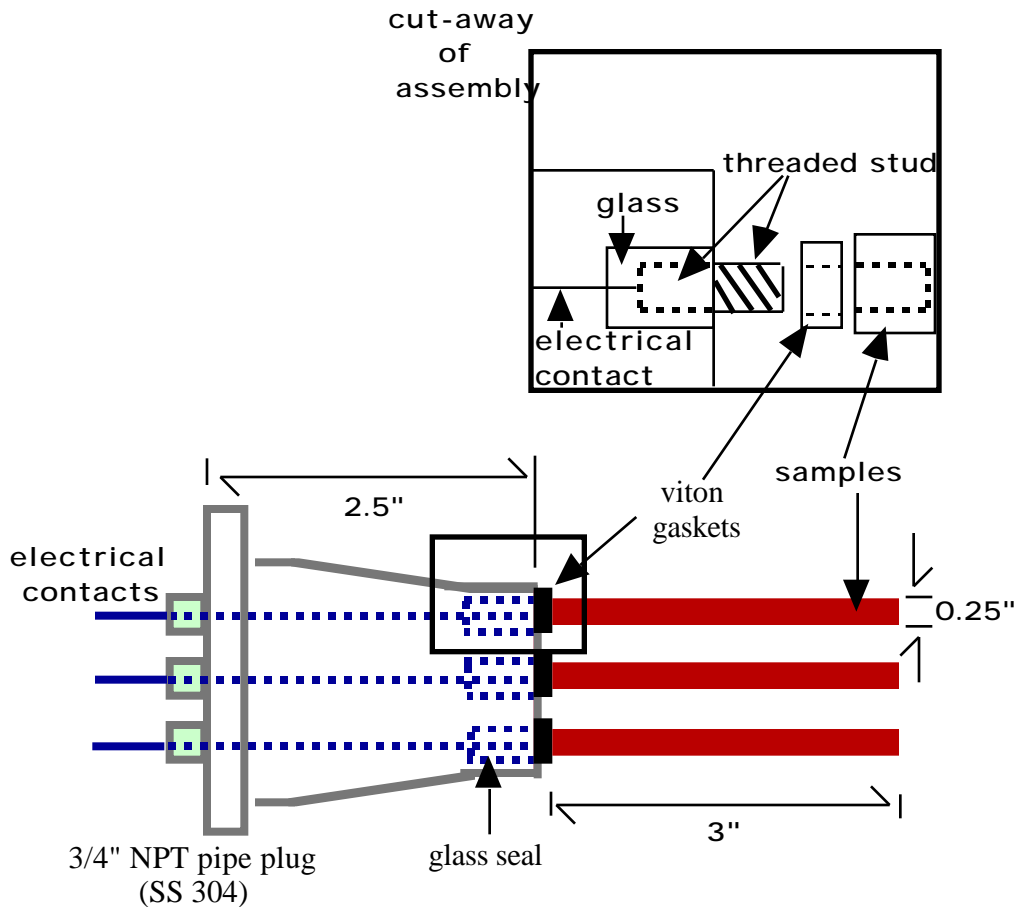


Figure 2 A diagram of the commercially available 3-electrode corrosion probes used in the LANSCE out-of-beam corrosion measurements.

and tantalum. The probe consisted of a 304 stainless steel NPT pipe plug style feedthrough that supported 3 threaded studs. These studs were joined to the feed through via a glass to metal seal that also provided electrical isolation. Each stud had a separate electrical contact. One end of the sample was tapped to accept the threaded stud. A water seal between the sample and glass was obtained via a Viton o-ring that was placed on each stud prior to screwing on the samples.

Prior to placing the corrosion samples on the probe, the surface was abraded with 600 grit SiC paper. The samples were then cleaned in an ultrasonic cleaner in successive baths of acetone, ethanol and DI water. A flame oxidized W sample was used for a

reference electrode (tungsten/tungsten oxide) and three C276 samples were used (together) as a counter electrode. The performance of the tungsten/tungsten oxide reference electrode is discussed below.

The final probes were fitted into corrosion cells (constructed from SS 304L) on both the supply and return sides of the cooling water loop at the top of the insert (approximately 12' from the proton beam). These cells contained an inlet and outlet for the system water and held approximately 8 liters of water. Although the water that flowed through these cells was activated (due to Be^7 and Co^{60} for example) and thus, exposed the samples to some level of radiation, the cells position allowed us to separate changes in corrosion rate due to proton irradiation from changes due to in solution water chemistry.

Conductivity Probes A modified version of the three electrode out-of-beam corrosion probes presented in Figure 2 above were used to measure changes in water conductivity. These conductivity were constructed by welding a hollow SS 304 tube onto two of the threaded sample mounting studs. This stainless steel sleeve surrounded a small stainless steel rod (also made from SS 304) which was welded onto the third sample mounting stud. This geometry allowed the probe cell constant (used to convert solution resistance to resistivity) to be determined more accurately than the configuration used in earlier experiments on the LANSCE XO2 cooling water system(13). One probe each was placed in the supply stream and one in the return stream at the top of the corrosion insert .

Hydrogen Water Chemistry In an attempt to mitigate the formation of hydrogen peroxide, Hydrogen Water Chemistry was used during the LANSCE irradiation experiments. This was accomplished by bubbling a mixture of H_2 / 94% Ar gas directly into the water reservoir. The dissolved hydrogen concentration in the cooling water loop during the LANSCE irradiation experiments was monitored with a remote hydrogen sensor, Orbisphere Laboratories, Emerson NJ, (model #3610/220.E, TCD Hydrogen Gas System). It has been shown for BWR / PWR reactors that the OCP is greatly suppressed during HWC(14, 15, 16, 17, 18, 19, 20).

Results and Discussions

OCP Measurements OCP measurements were made with respect to a W/W-oxide reference electrode. The OCP of the W/W-oxide electrode as a function of solution pH is shown in Figure 3. At pH 4.2, the pH of the water system, the OCP of the W/W-oxide electrode was -0.045 V relative to saturated calomel. Because the OCP of W/W-oxide changed only 0.03 V / pH unit, corrections for small pH deviations from a solution pH of 4.2 were not needed. Further, the OCP W/W-oxide electrode was independent of hydrogen concentration as shown in Figure 4 and only slightly dependent on H₂O₂ concentration.

The OCPs of the W and Ta probes as a function of immersion time are presented in Figure 5. As might be anticipated, the OCP of the W electrode is approximately 0 V vs W/W-oxide and remains fairly constant with time. Although a gradual increase in the OCP of most all samples was observed (Figures 6 and 7) which is consistent with an increase in the concentration of total oxidizing species (i.e., H₂O₂), in some cases the OCP of the samples followed one another more closely (i.e., the day 50 data for the Ta data in Figure 5 and the day 75 for the Fe/Ni alloys in Figure 6).

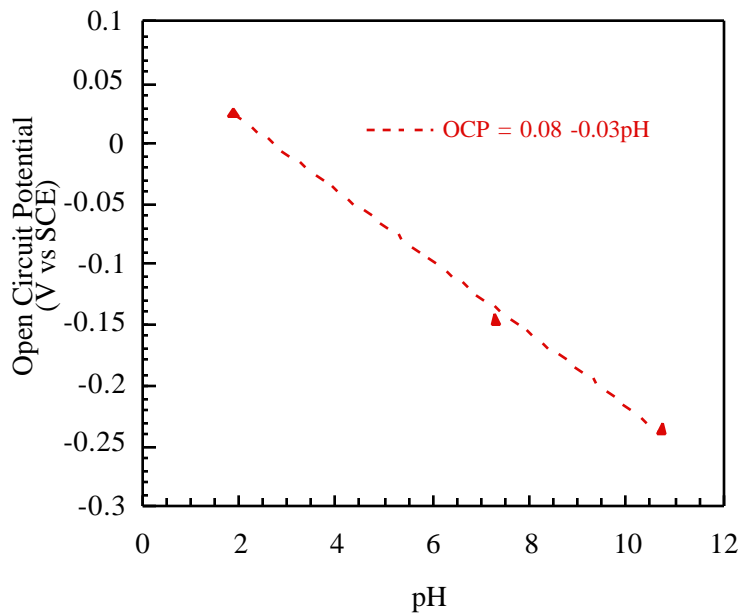


Figure 3 OCP of W/W-oxide electrode as a function of solution pH.

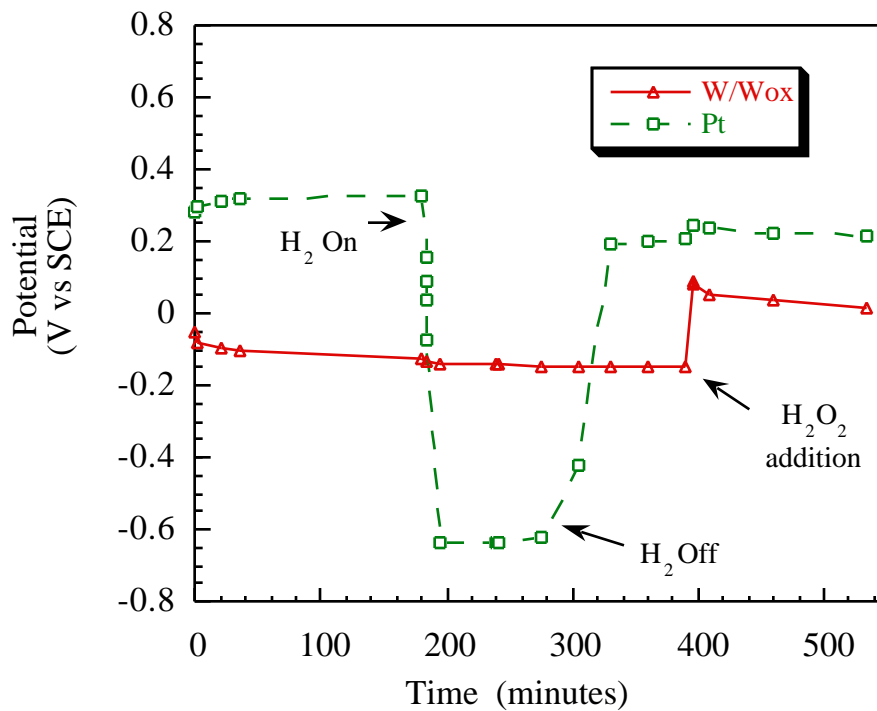


Figure 4 OCP of W/W-oxide and a Pt electrode as a function of time in boric acid / sodium borate buffer solution (pH 7). Plot shows the effect of H₂ and H₂O₂ additions.

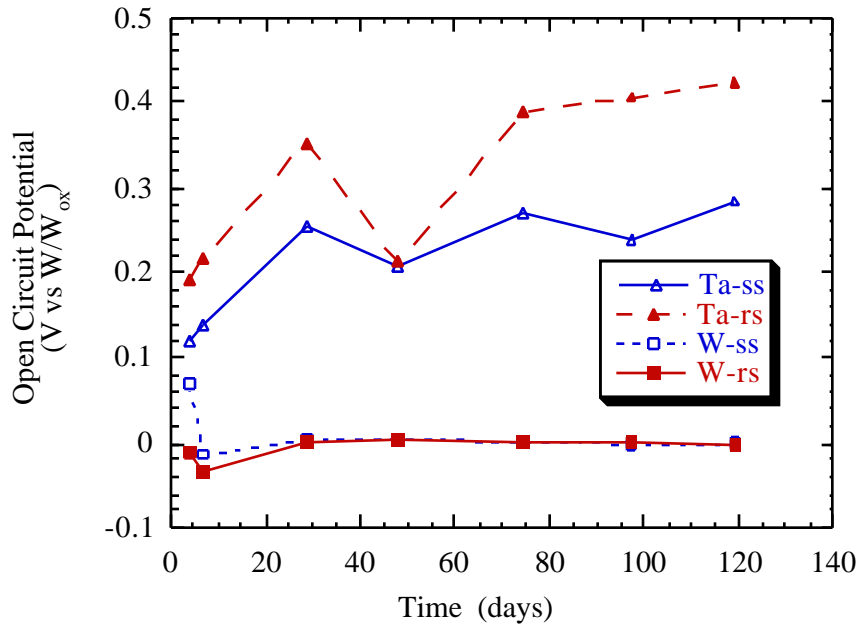


Figure 5 OCP of W and Ta electrodes in cooling water loop (supply and return electrodes) as a function of irradiation time.

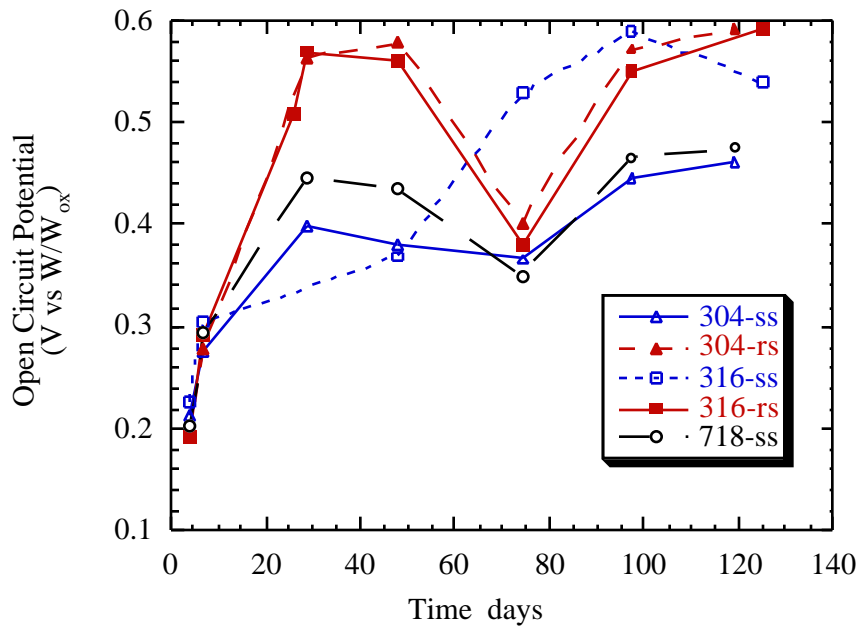


Figure 6 OCP of 304L, 316NUC, and 718 electrodes in cooling water loop (supply and return electrodes) as a function of irradiation time.

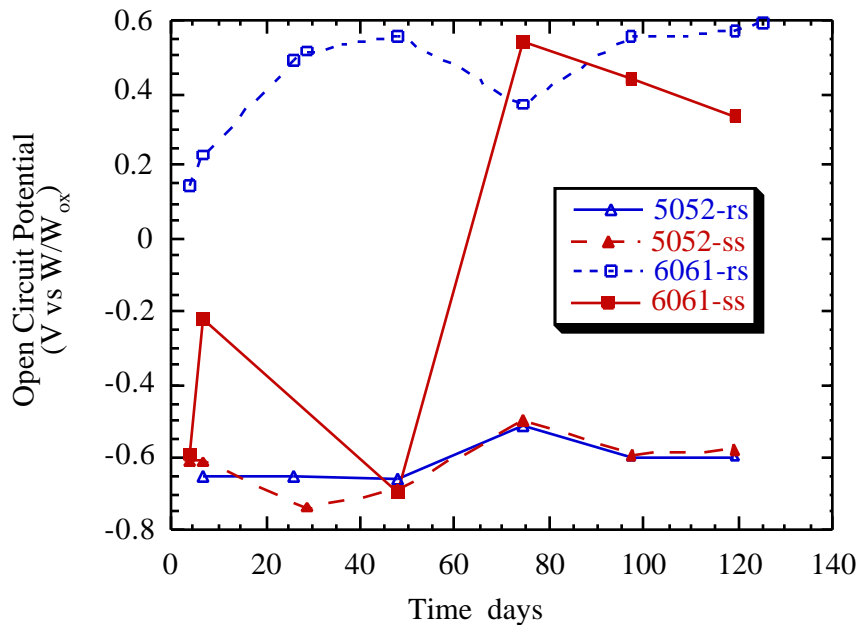


Figure 7 OCP of aluminum alloys 5052 and 6061 in cooling water loop (supply and return electrodes) as a function of irradiation time.

EIS Data and CNLS Modeling Typical EIS data for 718 and W are presented in Figures 8 and 9 at a proton beam current of 0.040 mA. EIS data for W as a function of beam current are presented in Figure 10. The figures are representative of those measured for all materials in this study at short to intermediate immersion times although the magnitude of the impedance was a function of material composition. The equivalent circuit (EC) model used to fit this data is presented in Figure 11a and is referred to as a Simplified Randle's Circuit. In this model R_{pol} represents the polarization resistance of the material, C_{dl} the double layer capacitance, and R_{sol} the geometric solution resistance between the working and reference electrodes. Typical curve fits of this model to the data are presented in Figures 8 and 9 as solid lines. As can be seen in these figures, good agreement between the model and the data exists. At longer immersion times a Warburg (diffusion) component in the EIS spectra of some samples was observed. For these data, the EC in Figure 11b

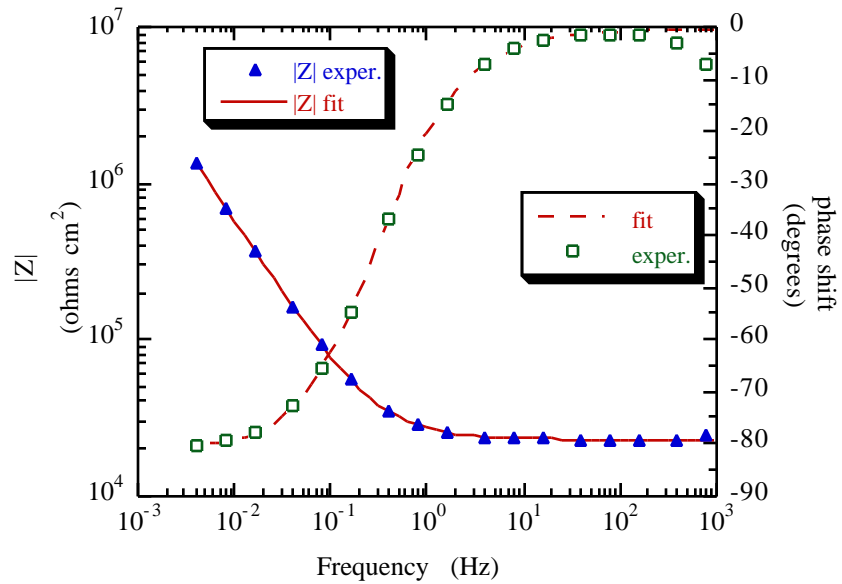


Figure 8 Bode magnitude and phase plots for the out-of-beam Inconel 718 probe (supply side). Proton beam current was 0.04 mA when these data were collected. Only a fraction of the experimental data is shown for clarity.

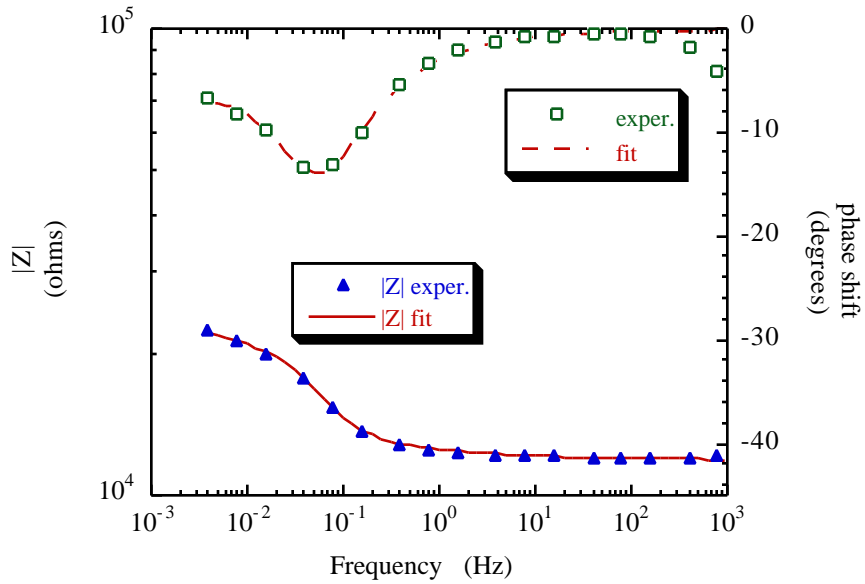


Figure 9 Bode magnitude and phase plots for the out-of-beam W probe (return side). Proton beam current was 0.04 mA when these data were collected. Only a fraction of the experimental data is shown for clarity.

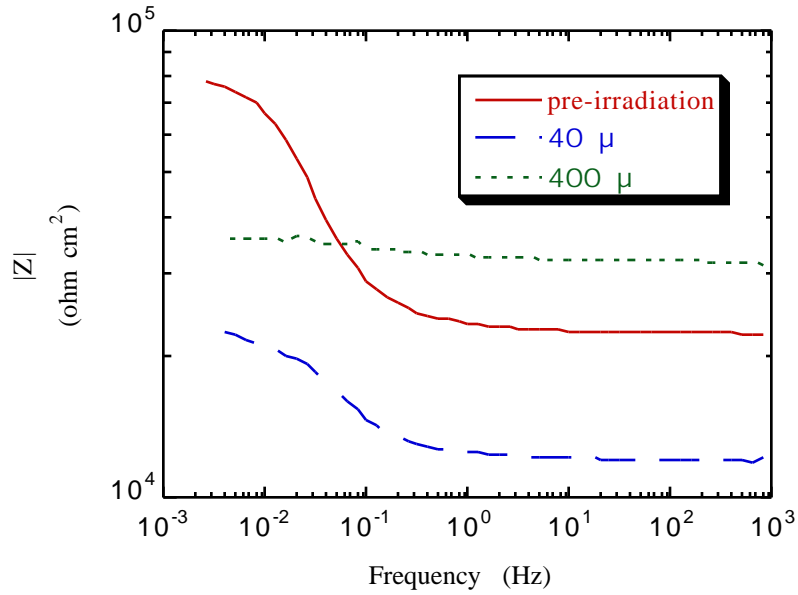


Figure 10a Bode magnitude plots for the out-of-beam W probe (return side) as a function of proton beam current.

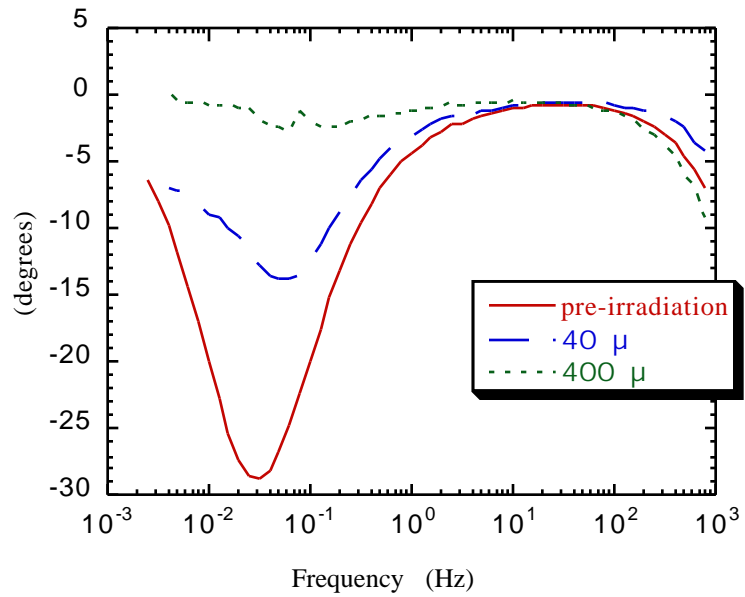


Figure 10b Bode phase plots for the out-of-beam W probe (return side) as a function of proton beam current.

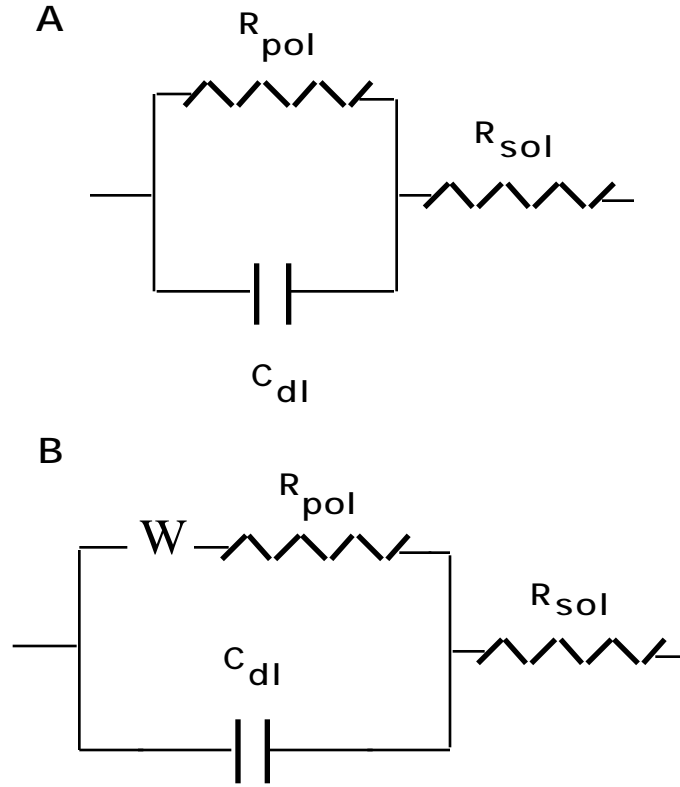


Figure 11 Equivalent circuits used to model EIS data: **a)** simplified Randle's circuit and **b)** diffusion impedance circuit.

was used to model the data. Once again, good agreement between the model and the experimental data exist.

Corrosion Rate vs Immersion Time From the values of R_{pol} , the corrosion rate of each sample was calculated as a function of immersion time. In these calculations i_{corr} was derived from R_{pol} by the Stern-Geary relationship(21):

$$i = 2.303i_{corr} \frac{a + c}{a c} (E_{ap} - E_{corr})$$

where: i is the applied current density, i_{corr} is the corrosion current density, E_{ap} is the applied potential, a and c are the anodic and cathodic Tafel slopes, and $i/(E_{ap} - E_{corr})$ is equal to $1/R_{pol}$. As the anodic and cathodic Tafel slopes for these materials in radiolyzed DI water was not known (and not easily determined) they were assumed to be 0.12V/decade current. It may be noted that the minimum and maximum allowable values for a and c

typically differ only by a factor of 3 (0.06 and 0.18V), therefore, $(E_{ap} - E_{corr})/i$ is more sensitive to changes in R_{pol} . From i_{corr} , the corrosion rate was determined from the well known expression:

$$CR_{mpy} = \frac{129(i_{corr}EW)}{\rho}$$

where: i_{corr} is in $A/cm^2 \times 10^{-3}$, EW is the equivalent weight in grms/equiv., and ρ is density in grms/cm³.

Caution is warranted when evaluating the following corrosion rates. The above calculations use corrosion current density and, therefore, yield a surface average rate and may not be conservative. Visual observation of the probe surface to examine for localized corrosion is necessary to confirm the following rates. In addition, in the absence of dissolved hydrogen (0.30 ppm here), rates will likely be higher.

The corrosion rate as a function of immersion time for each material type is presented in Figures 12 - 18. The proton beam status has been divided into three separate categories in these plots: 1) pre-irradiation, beam off, 2) beam on, 0.001-0.40 mA, corrosion insert only, and 3) beam on, 1 mA, all forward inserts in place. During early experiments when only the corrosion insert was in-beam, the beam spot at the corrosion manifold had a Gaussian distribution of $2\sigma = 3$ cm. With the forward inserts in place, because the proton beam first strikes 3 inserts before reaching the corrosion system the proton beam is no longer as focused at the corrosion insert, that is, 2σ at the corrosion manifold was greater than 3 cm. With respect to the corrosion rate of W (Figure 12), an increase in corrosion rate of the return side sample was observed at a proton beam current of 0.001 -0.40 mA. No change in the corrosion rate of the supply side probe was observed at these beam currents. Therefore, the observed increase in corrosion rate of the return side W probe is attributed to water radiolysis products that are either consumed or sufficiently diluted in the reservoir before reaching the supply side probe. The sharp

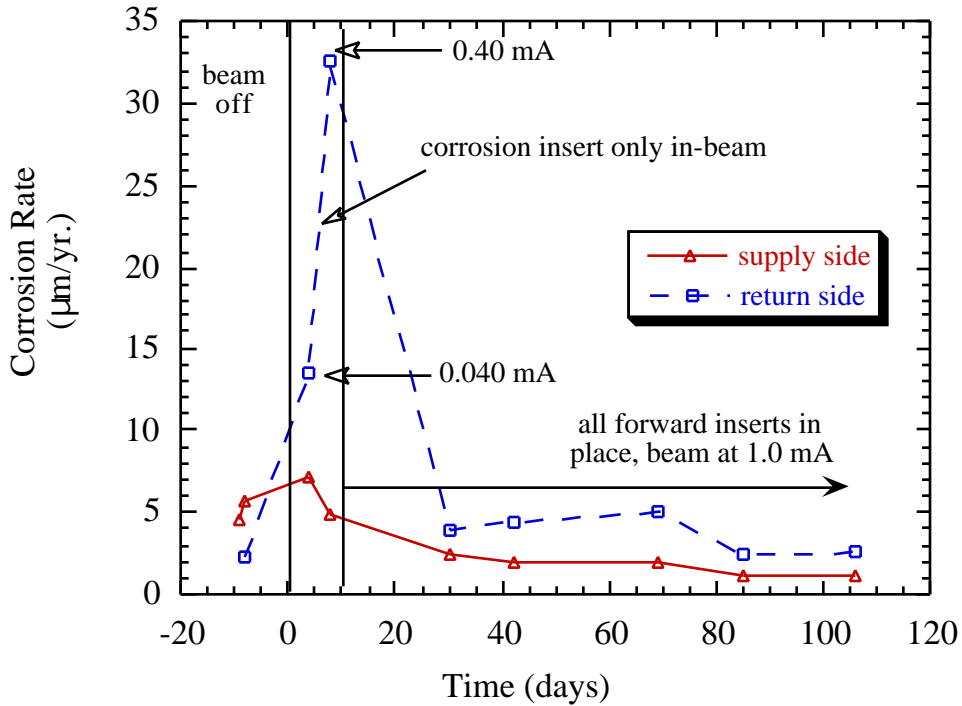


Figure 12 Corrosion rate for the tungsten corrosion probes as a function of immersion time.

decrease in corrosion rate observed between day 7 and 30 is likely due to the flush and refill of the water system that occurred on day 10.

For alloy 5052, changes in corrosion rate with immersion time appear to be similar for the return and supply side probes (Figure 13). Moreover the same trends are also observed in 6061 supply side probe (Figure 14). At early immersion times (pre-irradiation) the rates for both alloys were relatively high, probably due to inadequate cleaning of the water system. After flushing the water system and refilling it with DI water on day -7, the corrosion rates for both alloys decreased and remained low while the beam was ramped from 0.001 to 0.40 mA. At longer immersion times with the beam on at 1 mA, a peak in the corrosion rate around 40 days of immersion was observed in each probe except the return side Al 6061 probe which remained low. This peak was also observed in both W probes and may be due to water radiolysis products. Although one might anticipate that the concentration of radiolysis products would continually increase with time, a small leak in

the water system around day 40 resulted in additional DI water being added to maintain system pressure. Correspondingly, the concentration of radiolysis products was diluted thus explaining why the corrosion rate began decreasing after day 40.

With respect to the 304L, 316NUC, and 718 samples (7 samples in all, Figures 15-17), no trends in corrosion rate with immersion time were observed with the exception of the day 0 to 10 data. During this period a small increase in corrosion rate was observed in some of the probes as noted in the tungsten rates above. As for the remainder of the data, the corrosion rates of all of these samples were less than $0.12 \mu\text{m}/\text{yr}$ and, therefore, the observed fluctuations in corrosion rate with time may owe to inaccuracies in our measurement and modeling rather than real changes in corrosion rates.

Although the Ta corrosion rates were the lowest observed (Figure 18), the supply side rate increased independent of the proton beam current or flushing of the water system. Therefore, this trend is likely due to a change in the probe or sample integrity such as crevicing at the Viton gasket or failure of this gasket to adequately insulate the Ta sample from the probe assembly.

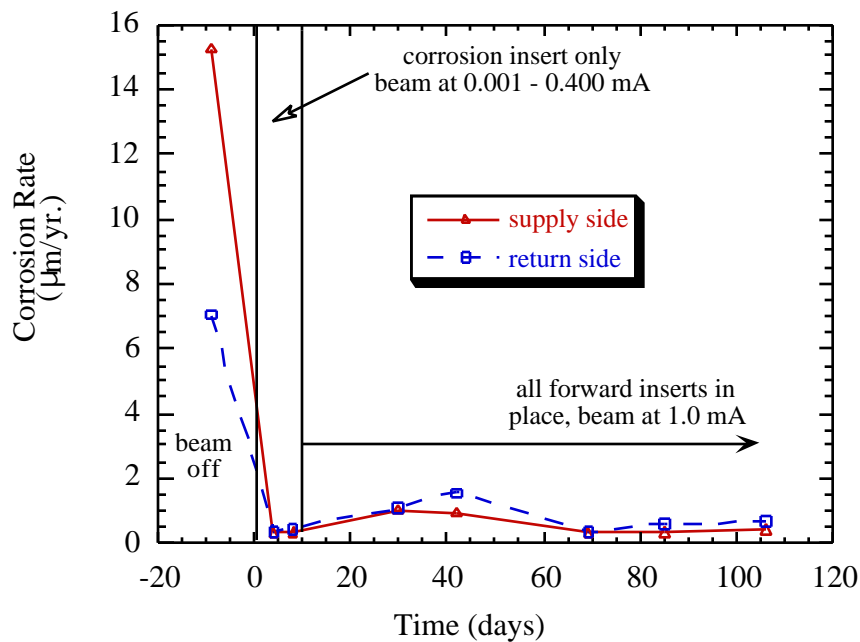


Figure 13 Corrosion rate for aluminum alloy 5052 corrosion probes as a function of immersion time.

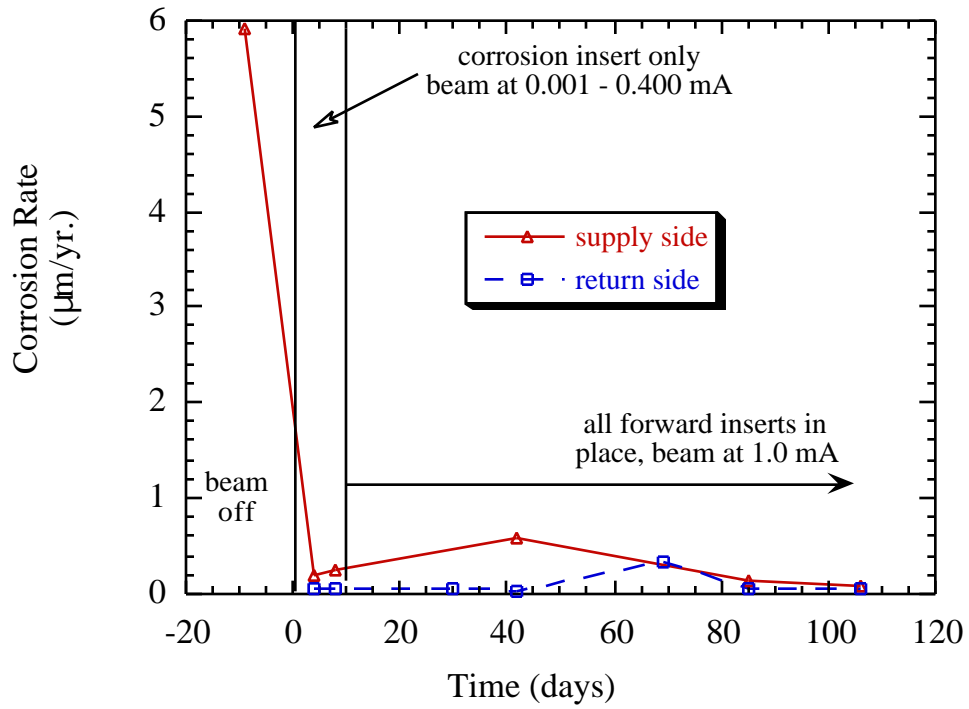


Figure 14 Corrosion rate for aluminum alloy 6061 corrosion probes as a function of immersion time.

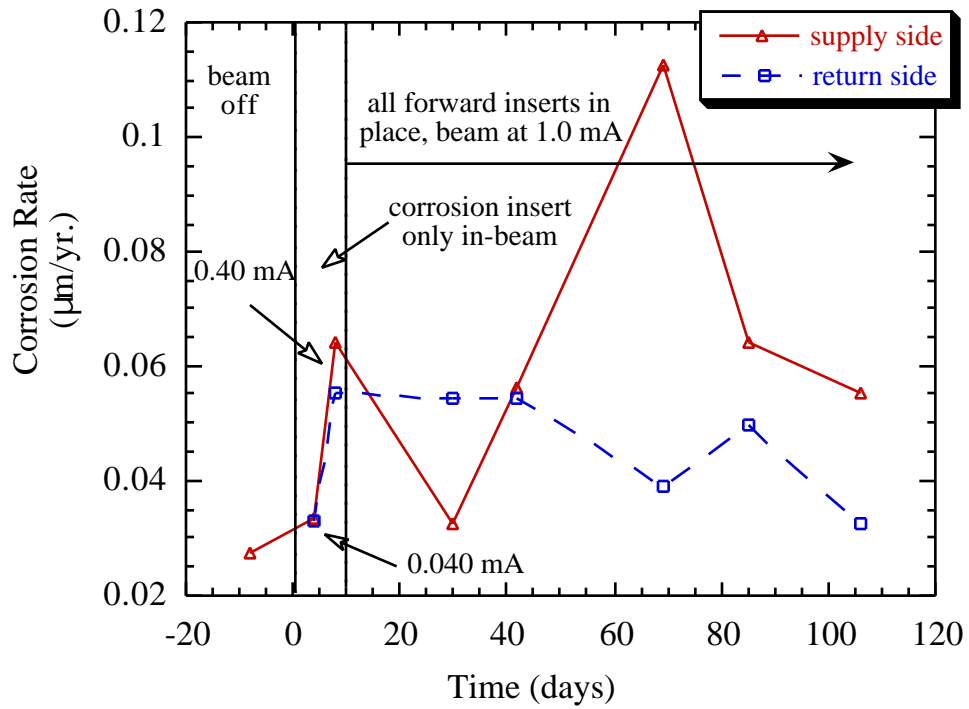


Figure 15 Corrosion rate for the stainless steel 304L corrosion probes as a function of immersion time.

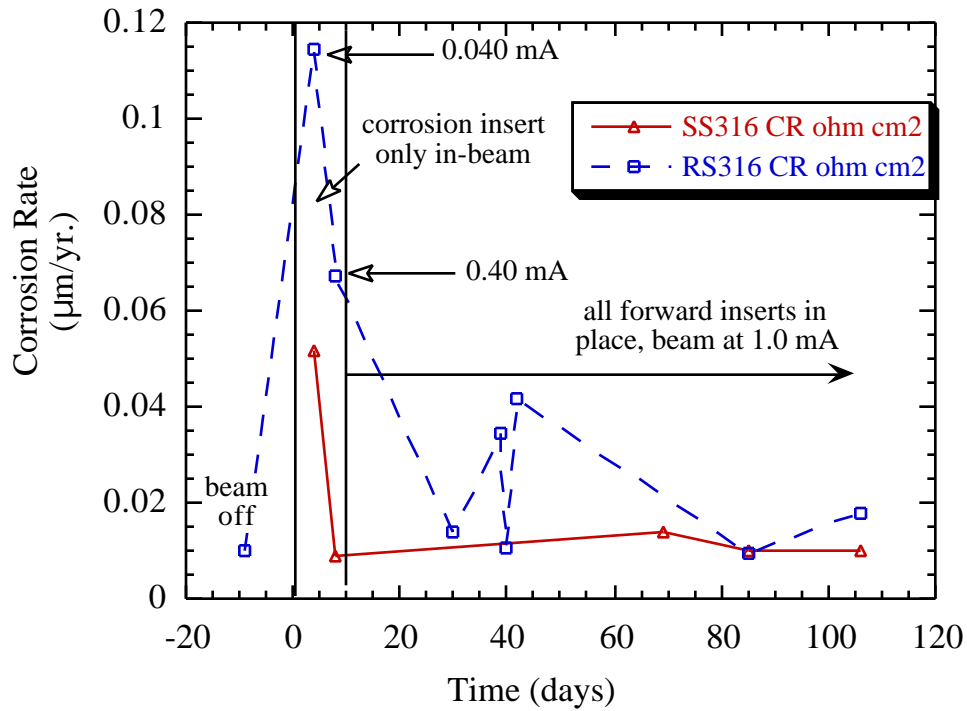


Figure 16 Corrosion rate for the stainless steel 316NUC corrosion probes as a function of immersion time.

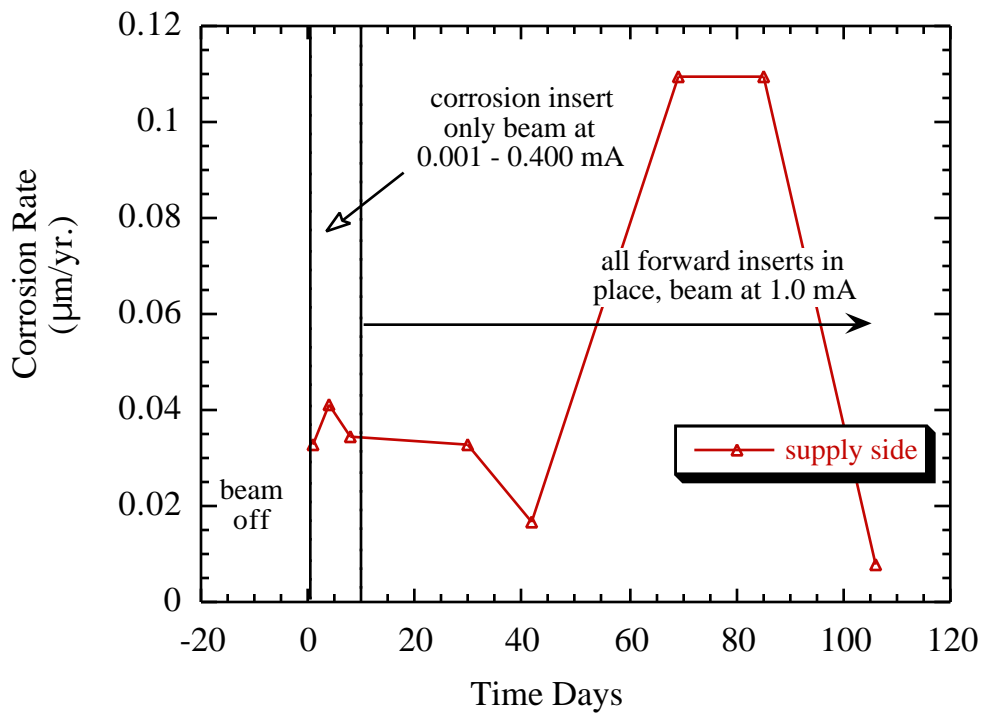


Figure 17 Corrosion rate for the supply side 718 corrosion probe as a function of immersion time. The return side probe did not pass our certification test.

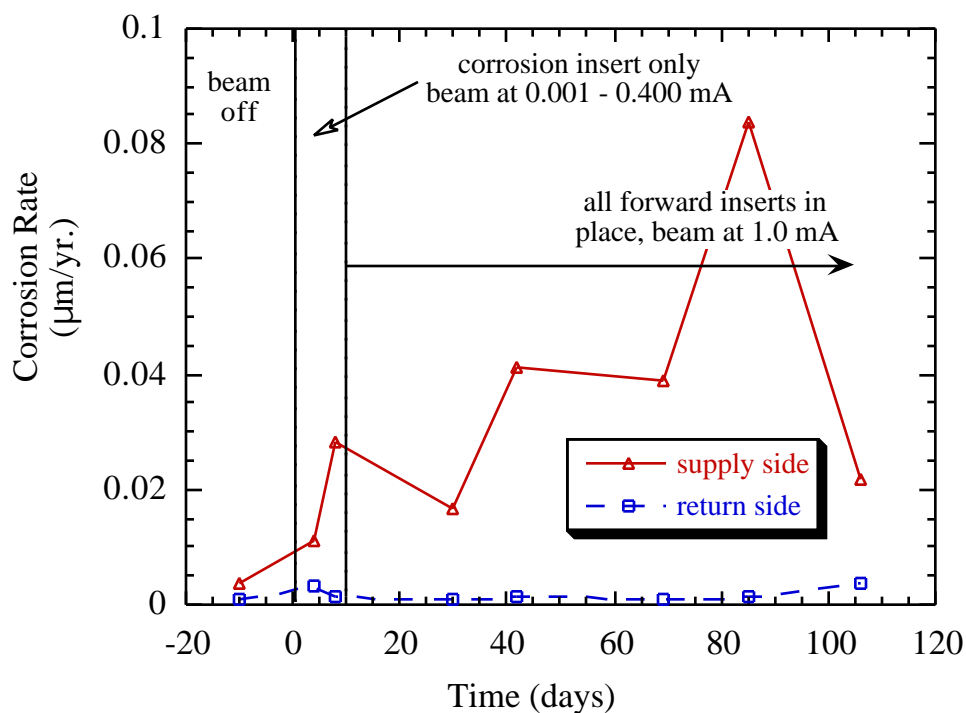


Figure 18 Corrosion rate for the tantalum corrosion probes as a function of immersion time.

Water Resistivity and Sampling Analysis The initial water resistivity for the corrosion water system was approximately 5×10^4 ohm·cm (Figure 19). The sharp decrease in water resistivity in the first several days before the beam was turned on likely owed to impurities that were being washed from the walls of the water system. Flushing the water system with fresh water and refilling it with additional DI water resulted in a sharp increase in water resistivity. The decrease in water resistivity observed when the proton beam current was increased from 0.4 mA to 1.0 mA likely owes to a combination of radiolysis and corrosion products. As shown in Table 2 an increase in water activity was observed. Gamma analysis of the water found that the water activity owing to water radiolysis (Be^7) and Fe/Ni alloy corrosion and radiolysis (Mn^{54} , Co^{56} , Co^{60}) increase with proton irradiation time. In addition, at the end of the irradiation period the concentration of H_2O_2 in the water system was 11.4 ppm. This concentration may have been greater had the system not leaked and/or the dissolved hydrogen concentration been lower.

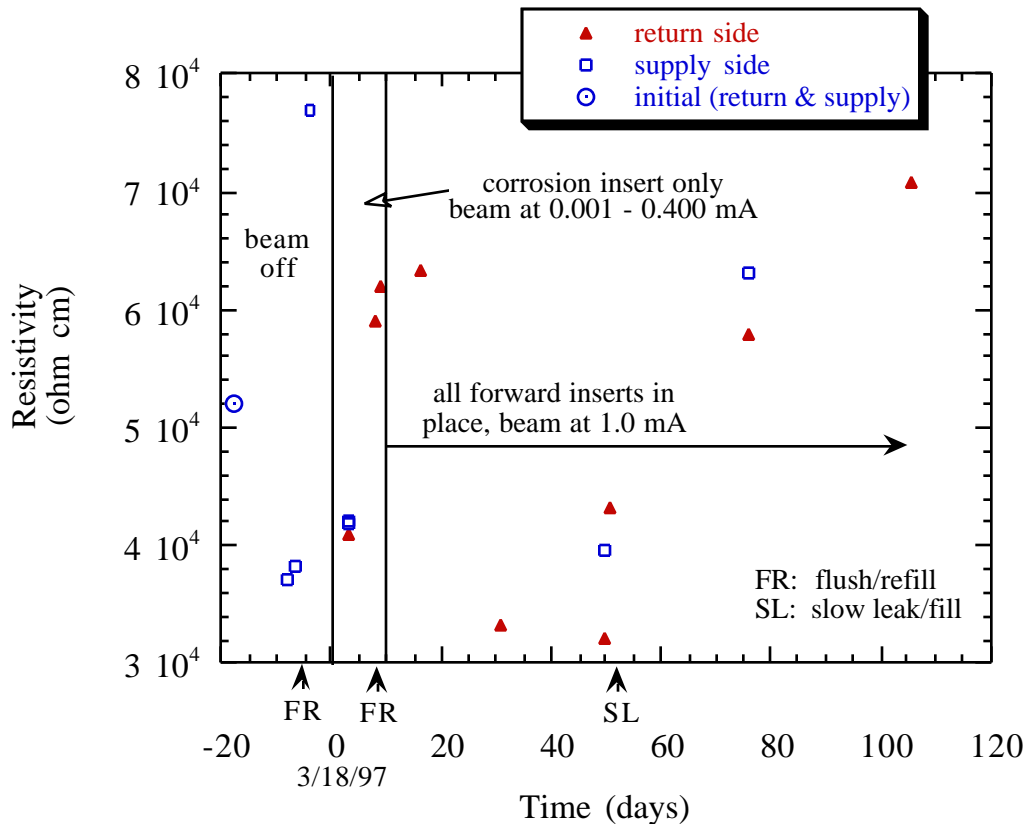


Figure 19 Water resistivity as a function of time from both the supply and return conductivity probes.

Table 2 Gamma and ICP analysis of water samples taken from the cooling loop as a function of time. Hydrogen peroxide concentration from paramagnetic titrations is also presented. The beam was turned on at day 0, therefore, negative days indicate the period before the beam was turned on. The abbreviation **nd** stands for non-detected.

days of beam	Gamma analysis (dpm)					ICP Analysis (ppm)				
	Be ⁷	Mn ⁵⁴	Sc ⁶⁴	Co ⁵⁶	Co ⁶⁰	W	Mg	Zn	Cu	Ca
-11	nd	nd	nd	nd	nd	0.01	0.03	0.04	0.02	2.6
	flush / refill system after day -6									
7	2.3 10 ⁴	100	nd	nd	nd	nd	0.13	0.45	0.04	2.9
	flush / refill system after day 7									
9	8.7 10 ⁴	400	178	nd	nd	0.06	0.05	0.19	0.04	1.9
66	4.0 10 ⁰	9.2 10 ⁵	465	7.4 10 ³	840	0.63	0.09	0.30	0.03	2.4
132	H ₂ O ₂ concentration = 11.4 ppm									

The trace impurities Mg, Zn, Cu, and Ca owe to the DI water as they were observed prior to turning the beam on and their concentration was not found to change greatly during the irradiation.

Summary

The corrosion rates for Inconel 718, stainless steels 304L and 316NUC, aluminum alloys 5052 and 6061, tantalum, and tungsten in water irradiated by the 800 MeV proton beam at the LANSCE A6 target station have been reported. These real-time corrosion rates were measured during the FY '97 irradiation period between March and July of 1997 in the APT-Corrosion water loop. The corrosion rates for stainless steels 304L and 316NUC, Inconel 718, and tantalum were extremely low, less than 0.12 $\mu\text{m}/\text{yr}$. Although visual inspection for areas of localized corrosion is necessary, from these results we conclude that the service lifetime of these materials in a deionized water, spallation neutron target cooling loop which employs hydrogen water chemistry would be extremely high, 20 years or more. As an example, for an Inconel 718 sample in a deionized water spallation neutron target cooling loop which employs hydrogen water chemistry the loss due to corrosion would only be less than 0.001" in a 10 yr. period. For comparison, the corrosion rate of an Inconel 718 sample placed directly in the proton beam has been shown in other investigations to be 0.002"/yr.

For aluminum alloys 6061 and 5052 the corrosion rates were slightly higher than the iron and nickel base alloys, on the order of 0.5 to 2.0 $\mu\text{m}/\text{yr}$. However, the service lifetime of these materials in a deionized water, spallation neutron target cooling loop which employs hydrogen water chemistry is expected to be comparable to that of the stainless steels.

Relative to the other materials tested in this investigation, the corrosion rate of tungsten was found to be high, between 5 and 30 $\mu\text{m}/\text{yr}$. However, in a 10 yr. period the total loss of W in a deionized water, spallation neutron target cooling loop which employs hydrogen water chemistry would only be 0.002" - 0.012". For comparison, the corrosion

rate of a tungsten sample placed directly in the proton beam has been shown in other investigations to be greater than 0.060"/yr.

The effects of proton irradiation on water quality have also been investigated. Water resistivity decreased from approximately 5×10^4 to a value of 3×10^4 ohm·cm in the first several days of operating the system before the beam was turned on. At that time the system water was drained, the system was flushed and refilled with fresh deionized water and, as anticipated, an increase in resistivity was observed. The largest decrease in resistivity were observed when the beam proton beam was turned on. Gamma analysis of the water as a function of irradiation time found that the water activity owing to water radiolysis (Be^7) and Fe/Ni alloy corrosion and radiolysis (Mn^{54} , Co^{56} , Co^{60}) increased with proton irradiation time. ICP analysis of these water samples found trace impurities of Mg, Zn, Cu, and Ca, however, these were believed to come from the DI water as they were observed prior to turning the beam on and their concentration was not found to change greatly during the irradiation. At the end of the irradiation period the concentration of H_2O_2 in the water system was 11.4 ppm. This concentration may have been greater had the system not leaked and/ or hydrogen water chemistry not been implemented.

References

1. R. S. Lillard, D. L. Pile, D. P. Butt, "Materials Corrosion and Mitigation Strategies for APT, End of FY '97 Report: I. Inconel 718 In-Beam Corrosion Rates from the '97 A6 Irradiation" *LAUR-98-0764* (Los Alamos National Laboratory, 1997).
2. T. K. Yeh, D. D. MacDonald, A. T. Motta, *Nuclear Science and Engineering*, **121**, 468 (1995).
3. H. Christensen, *Nuclear Technology*, **109**, 373 (1994).
4. J. L. Magee, A. Chatterjee, in *Kinetics of Nonhomogeneous Processes*, G. R. Freeman, Ed., p. 171, John Wiley & Sons, New York (1987).
5. W. G. Burns, P. B. Moore, *Radiation Effects*, **30**, 233 (1976).
6. R. S. Glass, G. E. Overturf, R. A. V. Konynenburg, R. D. McCright, *Corrosion Science*, **26**, 577 (1986).
7. Y. J. Kim, R. A. Oriani, *Corrosion*, **43**, 92 (1987).
8. Y. J. Kim, R. A. Oriani, *Corrosion*, **43**, 85 (1987).
9. G. Capobianco, G. Palma, G. Granozzi, A. Glisenti, *Corrosion Science*, **33**, 729 (1992).
10. I. Epelboin, C. Gabrielli, M. Keddam, H. Takenouti, in *Electrochemical Corrosion Testing, ASTM STP 727*, F. Mansfeld, U. Bertocci, Eds., p. 150, ASTM, Philadelphia (1981).
11. J. R. MacDonald, *Impedance Spectroscopy*, Wiley Publishing, New York (1987).
12. D. D. MacDonald, in *Electrochemical Corrosion Testing, ASTM STP 727*, F. Mansfeld, U. Bertocci, Eds., p. 110, ASTM, Philadelphia (1981).
13. R. S. Lillard, D. P. Butt, "Preliminary Spallation Neutron Source Corrosion Experiments: Corrosion Rates of Engineering Materials in a Water Degraded Cooling Loop Irradiated by an 800 MeV Proton Beam" *LA-UR 96-1011* (Los Alamos National Laboratory, 1996).
14. M. E. Indig, J. E. Weber, . (NACE, Houston, TX, 1983).

15. W. R. Kassen, R. P. Jones, J. L. Tollefson, . (NACE, Houston, TX, 1992).
16. M. Fox, . (NACE, Houston, TX, 1983).
17. C. C. Lin, R. L. Cowan, R. S. Pathania, . (NACE, Houston, TX, 1993).
18. L. G. Ljungberg, D. Cubicciotti, M. Trolle, . (NACE, Houston, TX, 1985).
19. M. J. Fox, “A Review of Boiling Water Reactor Chemistry: Science, Technology, and Performance” *NUREG/CR-5115 ANL-88-42* (Argonne National Laboratory for the US Nuclear Regulatory Commission, 1989).
20. Y. J. Kim, . (NACE, Houston, TX, 1996).
21. J. O. M. Bockris, A. K. N. Reddy, *Modern Electrochemistry, Volume 2*, Plenum Publishing Corp., New York (1973).